PROGRESS IN PHOTOVOLTAICS: RESEARCH AND APPLICATIONS
Prog. Photovolt: Res. Appl. 2008; **16**:297–305
Published online 22 January 2008 in Wiley InterScience (www.interscience.wiley.com) DOI: 10.1002/pip.812

Research

Luminescence Imaging for the Detection of Shunts on Silicon Solar Cells

M. Kasemann[1]*,†, D. Grote[2], B. Walter[2], W. Kwapil[2], T. Trupke[3], Y. Augarten[3], R.A. Bardos[3], E. Pink[3], M.D. Abbott[3] and W. Warta[2]

[1]*The University of Freiburg, Material Research Center, Stefan-Meier-Str. 21, 79104 Freiburg, Germany*
[2]*Fraunhofer Institute for Solar Energy Systems (ISE), Heidenhofstr. 2, 79110 Freiburg, Germany*
[3]*Centre of Excellence for Silicon Photovoltaics and Photonics, The University of New South Wales, Sydney 2052, New South Wales, Australia*

Luminescence imaging is a non-destructive, fast, and versatile imaging method for spatially resolved solar cell and material characterization. In this paper, we investigate its ability to detect shunts on silicon solar cells. We give a detailed description of the relation between local junction voltage and local luminescence signal. This relation is important because shunts drain majority currents causing voltage drops across the surrounding series resistances and that way affect luminescence images. To investigate effects related to majority currents, we describe and apply a simulation model that allows the simulation of lateral voltage distributions on solar cells. This model, and a comparison to illuminated lock-in thermography, helps to discuss some practical aspects about shunt detection by luminescence imaging. We will discuss a procedure to distinguish between ohmic and diode-like shunts and finally present simulations and measurements showing that luminescence imaging is only weakly sensitive to shunts under the metallization. However, we also show its high sensitivity for remote shunts and propose a possible application where this high sensitivity could be especially helpful. Copyright © 2008 John Wiley & Sons, Ltd.

KEY WORDS: luminescence imaging; shunt detection; silicon solar cell characterization

Received 31 August 2007; Revised 19 November 2007

INTRODUCTION

Electroluminescence (EL) and photoluminescence (PL) imaging are novel tools for non-destructive and fast spatially resolved silicon solar cell characterization.[1,2] Typical measurement times of around 1 s could allow for an in-line application of these techniques in silicon solar cell production. First applications of luminescence imaging to shunting problems have already been reported.[3–5] In this paper we present experiments and detailed theory on the application of luminescence imaging for shunt detection on silicon solar cells. The shunt detection capabilities of luminescence imaging methods are investigated by one-dimensional semiconductor simulations, electrical circuit simulations, and are compared to lock-in thermography methods which have already been extensively used to localize and classify shunts.[6–11]

Section 'Description of measurement methods and simulation model' gives an overview of the theory behind luminescence imaging with an emphasis on the relation between local junction voltage and local

* Correspondence to: M. Kasemann, The University of Freiburg, Material Research Center, Stefan-Meier-Str. 21, 79104 Freiburg, Germany.
†E-mail: martin.kasemann@fmf.uni-freiburg.de

luminescence signal in a one-dimensional model. We will continue with a short recapitulation of the ILIT method and with the description of a simulation model used to simulate the influence of lateral majority currents on the voltage distribution on the cell, which relates to the appearance of luminescence images. Section 'Simulation and measurement results and discussion' presents simulation and measurement results, starting with a discussion on how shunts appear in luminescence images. Then we will turn to a more practical aspect and discuss a procedure to distinguish between ohmic shunts and diode-like shunts which is non-trivial with luminescence imaging. Finally, we present simulations and measurements that show a fundamental limitation of luminescence imaging connected with the detection of shunts below metallization. However, we also demonstrate high sensitivity of luminescence imaging for remote shunts and propose a possible application where this high sensitivity could be particularly helpful.

DESCRIPTION OF MEASUREMENT METHODS AND SIMULATION MODEL

Luminescence imaging

The luminescence photons, which are detected in luminescence imaging, are generated by band-to-band electron-hole recombination within a semiconductor device.[12] The radiative recombination rate in a silicon solar cell under typical operating conditions is sufficient to allow for a spatially resolved detection of luminescence radiation by a cooled silicon charge-coupled device (CCD) camera. In the PL imaging setup used in this study, we realize full area illumination over $125 \times 125\,\mathrm{cm}^2$ by an 804 nm diode laser with the photon flux density comparable to 0.7 suns under AM 1.5 conditions. For EL measurements and for PL measurements under load conditions, the cell can be electrically contacted.

The local luminescence signal S_{xy} is given by (compare e.g. References 4, 12)

$$S_{xy} = C \cdot \int_0^d \frac{n_{xy}(z)p_{xy}(z)}{n_i^2}\,\mathrm{d}z = C \cdot \int_0^d \exp\left[\frac{\Delta\eta_{xy}(z)}{\mathrm{k}T}\right]\mathrm{d}z \qquad (1)$$

where C is a calibration constant, z the depth-distance from the front surface, d the thickness, n_{xy} and p_{xy} the electron and hole concentration, respectively, n_i the intrinsic carrier concentration, and $\Delta\eta_{xy}(z)$ the depth-dependent difference between the quasi-Fermi-levels below a surface-element at pixel position (x,y) on the sample. Equation (1) does not account for reabsorption of luminescence photons.[13] This effect has negligible influence on our conclusions and on the shape of the curves presented later. For completeness, however, all curves given later are calculated including reabsorption similar to the comprehensive treatment in Reference 13.

Only under special conditions can the local PL intensity S_{xy} be related to the local junction voltage V_{xy} in a simple way as in References 3, 14, assuming a constant product of the carrier densities $n_{xy}p_{xy}$ and thus constant $\Delta\eta_{xy} \approx \mathrm{e}V_{xy}$ over the entire depth z. This is only a good approximation as long as the local minority carrier diffusion length is much larger than the thickness of the cell, the back-surface recombination velocity is low, and the separation of the quasi-Fermi-levels is not significantly reduced toward the junction. In a more realistic scenario, bulk recombination and back surface recombination reduce the charge carrier density toward the back of the cell and also the p–n-junction has a detrimental influence on the carrier density profile, depending on the junction voltage. If the minority carrier distribution in the base is solely controlled by diffusion into the base as for EL and for PL with very short-wavelength irradiation (both under low-injection conditions), it is not necessary to assume a constant carrier density product $n_{xy}p_{xy}$ over the entire depth of the cell to obtain a proportionality between luminescence signal S_{xy} and $\exp(\mathrm{e}V_{xy}/\mathrm{k}T)$. In these cases, it is sufficient to have injection-level-independent minority carrier recombination and transport parameters. The proportionality is then a direct conclusion of the linearity and homogeneity of the excess carrier continuity equation in the absence of excess carrier generation in the bulk. We assume the p–n-junction, the surface of irradiation incidence in the PL case, and the detection side to be on the front side of the cell.

To illustrate and extend the above considerations, Figure 1a shows depth-dependent carrier profiles for different junction voltages under illuminated (PL) and dark (EL) conditions. The profiles have been simulated by PC1D.[15] For PL, the illumination intensity was held constant and the junction voltage was varied. While the carrier distribution in the dark is always governed by

DOI: 10.1002/pip

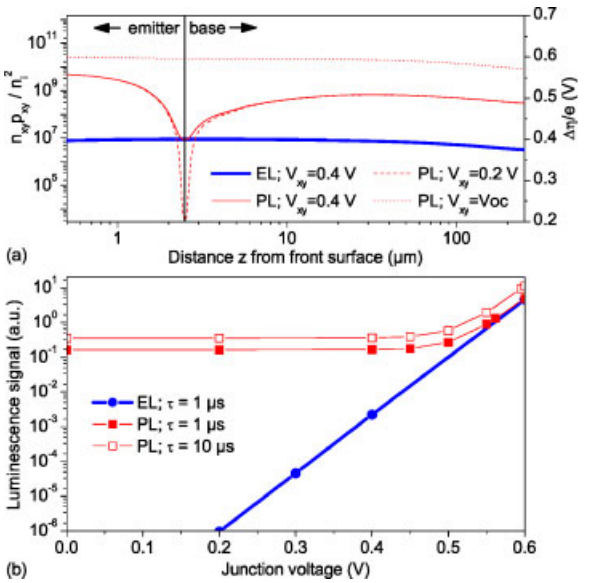

Figure 1. (a) Simulated depth-dependence of the splitting of the quasi-Fermi-levels $\Delta\eta_{xy}(z)$ for different junction voltages. The three curves labeled PL are calculated for constant illumination with monochromatic 804 nm light with an intensity of 0.0441 W/cm^2 (corresponding to a photon flux density of 0.7 suns) and variable junction voltage. (b) Simulated intensity of the luminescence signal depending on the local junction voltage V_{xy} for EL and PL and different minority carrier lifetimes τ. The curves include reabsorption according to Reference 13 with the spectral response of our camera and our filter setup. The PC1D[15] simulations were performed with a 250 μm thick p-type base with base doping of 10^{16} cm^{-3} and a complementary error function emitter profile with peak doping of 2.159×10^{19} cm^{-3} and a junction depth of 2.476 μm (40 Ω/□). Front and rear surface recombination velocity were set to 10^4 cm/s and 300 cm/s (back surface field), respectively. The carrier mobility in the base was 1107 cm^2/Vs for electrons and 424.6 cm^2/Vs for holes

the junction voltage for a given minority carrier lifetime, the carrier distribution under illumination is governed by light absorption. For low junction voltages, the shape of the excess carrier distribution in the bulk is independent of the junction setting (diffusion limited carrier distribution) as long as there is an appreciable optical generation within the base. These observations lead directly to Figure 1b, where we calculated the resulting luminescence signal from the simulated charge carrier distributions according to Equation (1) and Reference 13. In the dark case, the EL signal follows the junction voltage exponentially under forward bias. Under illumination, however, the PL intensity remains almost constant toward low voltages while it follows the junction voltage exponentially for voltages close to and above open-circuit voltage. The theoretically predicted constant luminescence intensity toward low voltages was recently observed experimentally.[16] We also included a calculation for two different minority carrier lifetimes into Figure 1b to illustrate the signal reduction caused by the back-side tail of the carrier distribution.

The relation between luminescence intensity and local junction voltage is the reason why localized shunts (and series resistances) can be detected by luminescence imaging methods. As will be shown in detail later, localized shunts drain majority currents from the surrounding regions of the cell, eventually causing a voltage drop across the series resistances which connect the shunt laterally to the surrounding non-shunted areas. This voltage drop leads to a "blurred" intensity dip around the position of shunts which has been observed in luminescence images.[3,5,17–19] A future quantification of shunt resistances (and series resistances) from luminescence images will rely on an accurate knowledge of the relation between local junction voltage and local luminescence signal. The above discussion shows that a voltage calibration is potentially easier for EL images than for PL images around the positions of shunts because the luminescence signal follows the junction voltage exponentially also toward low voltages (if lateral in-diffusion of minority carriers is small, see Section 'A model for the simulation of voltage distributions around shunts'). For PL images, a voltage calibration and quantitative evaluation of shunt resistances is more complex because of the diffusion limited carrier distribution for voltages significantly smaller than the open-circuit voltage. As will be shown in simulations later, the voltage dips around localized shunts can easily lead to low local junction voltages in the shunted region where the luminescence intensity can be strongly affected by this effect.

To predict the local voltage more accurately from the PL intensity, it was thus recently proposed that the PL intensity measured at a given operating point minus the constant PL intensity measured at low voltages could be a more reliable indicator of the local junction voltage.[16] This proposal remains to be verified theoretically and experimentally which is beyond the scope of this paper. For the discussion in this paper, it is sufficient to keep in mind that the EL and PL signal is related to the junction voltage qualitatively in a manner as indicated in Figure 1b.

DOI: 10.1002/pip

Shunt detection with illuminated lock-in thermography

Lock-in thermography is a non-destructive method to image lateral power loss distributions on solar cells under different injection conditions. If the measurements are performed under current injection in the dark, the method is called dark lock-in thermography (DLIT), while DLIT with additional illumination of the cell is called illuminated lock-in thermography (ILIT). In both cases, the images are taken by a cooled CCD camera, sensitive in the wavelength range of 3–5 μm using a lock-in procedure for noise reduction and reduction of lateral heat spreading effects.[11] Different power loss mechanisms in solar cells are accessible by setting different irradiation conditions and electrical load conditions on the cell. The scale of the ILIT images displayed in this contribution is proportional to the locally dissipated power.[8,9] In our ILIT setup, we realize full area irradiation by a widened 940 nm diode laser with a photon flux density set to 0.7 suns to be comparable to the luminescence imaging setup. The cell can be electrically contacted by four-point probes. Further details about the ILIT setup, which is more complex than the luminescence system because of the use of the lock-in analyzer, can be found in References 8, 11.

If ILIT measurements are performed under open circuit conditions, the resulting images are dominated by bulk and depletion region recombination heat and Joule heating in shunts.[7,8,20] In contrast to luminescence imaging and important in this context is, that local shunts and recombination centers are additional heat sources and thereby radiation sources *themselves*.[3] The electrical power dissipated in shunts is the product of local electrical current and local voltage.

A model for the simulation of voltage distributions around shunts

A means to simulate effects related to lateral majority current flows in solar cells are electrical circuit simulations.[3,21–24] For our simulations, we use a software tool based on SPICE.[25] Figure 2 sketches the basic idea behind the simulation model which is similar to models already described before.[3,21–24] The solar cell is divided into a large number of elementary units, each representing a certain volume element of the cell. Depending on the local properties (e.g. local shunts, shaded areas, etc.), elementary units are composed of a current source representing the light-generated current, two diodes with ideality factors one and two, respectively, and a parallel resistance representing an ohmic shunt. The elementary units are interconnected by a series resistance network representing the emitter sheet resistance, emitter-metal contact resistance and metallization resistance.

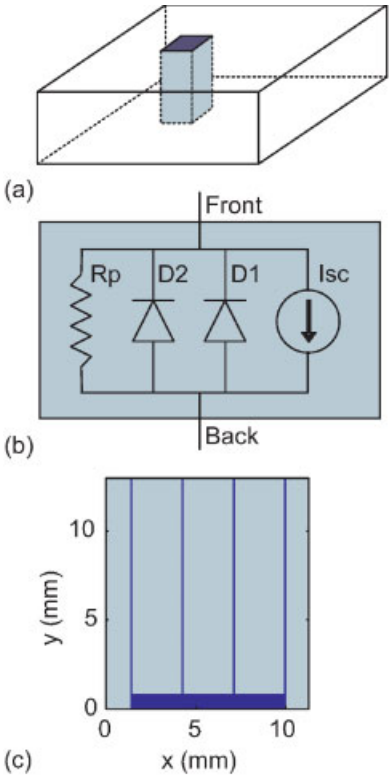

Figure 2. Circuit simulation model for the simulation of majority currents in silicon solar cells. (a) An elementary unit represents a certain volume element of the solar cell. (b) Every elementary unit is composed of a current source, diodes with ideality factors one and two, and a parallel resistance representing a shunt. The actual setup of elementary units can vary for example, if there is a local shunt or a shaded area. The elementary units are interconnected by a series resistance network representing the emitter sheet resistance, emitter–metal contact resistance and metallization resistance. (c) Grid design and dimensions of the simulated sample solar cell. The dimensions are 11.8 mm in x-direction and 13.0 mm in y-direction, with a node size of $63 \times 63\ \mu m^2$. In this setup we have two elementary units below a grid finger and 45 elementary units between two grid fingers in x-direction

To investigate the influence of localized shunts on the appearance of luminescence images, we simulated a small solar cell with high spatial resolution. The cell dimensions are 11.8 mm in x-direction and 13.0 mm in

DOI: 10.1002/pip

y-direction. Grid finger spacing and emitter sheet resistance are comparable to industrial solar cells. The node size is $63 \times 63\,\mu m^2$ allowing to set two elementary units below a grid finger and 45 elementary units between two grid fingers in x-direction. Localized shunts are modeled as one elementary unit implementing a shunt resistor or a shunt diode parallel to the diodes and the current source.

Please note that we neglect lateral minority carrier currents in these simulations. Recent results obtained in connection with diffusion length measurements using EL imaging have indicated that additional effects due to lateral minority carrier diffusion in the bulk can be observed by luminescence imaging in the vicinity of localized shunts, once the strong effects caused by majority currents have been eliminated experimentally.[26] Including minority carrier diffusion effects into simulations would require three-dimensional simulations which are beyond the scope of this approach and which remain to be performed in the future.

SIMULATION AND MEASUREMENT RESULTS AND DISCUSSION

The influence of majority currents on luminescence images—the voltage dip

We already stated that the majority carrier currents drained by the shunt cause a voltage dip which is detectable by luminescence imaging. Figure 3a illustrates qualitatively the appearance of PL images around localized shunts with different shunt resistances (from left to right 40 Ω, 160 Ω, and 640 Ω, respectively). The qualitative local luminescence signal was calculated from the local voltage V_{xy} by

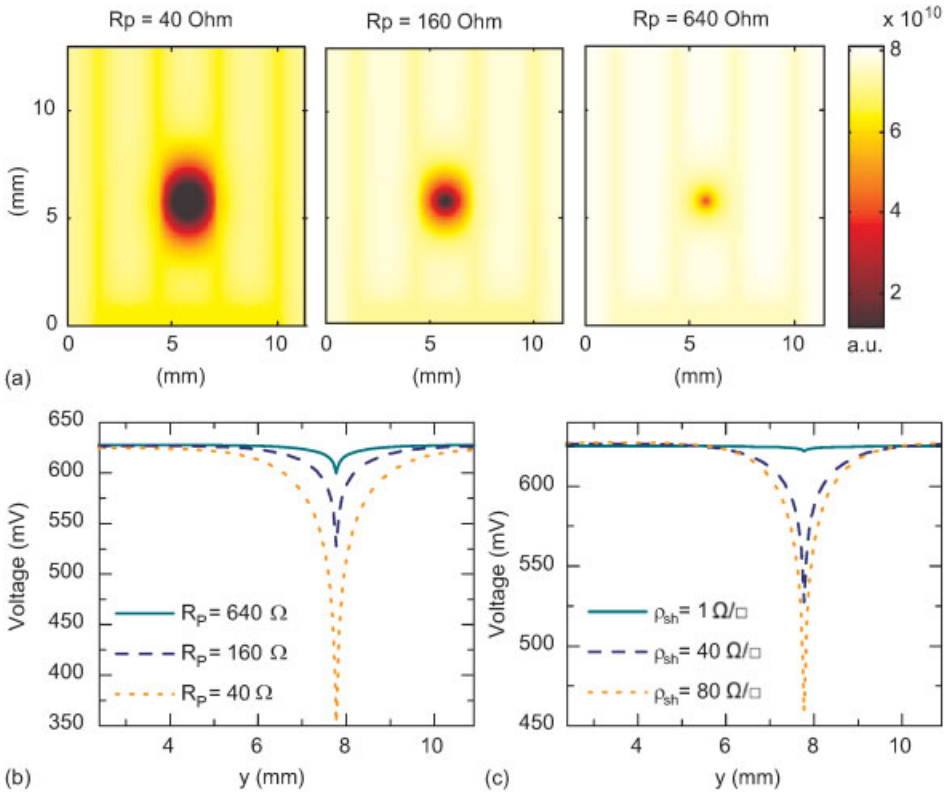

Figure 3. Circuit simulations of (a) PL images for different shunt resistances which were calculated from the voltage V by $\exp(eV/kT)$ with $kT/e = 25$ mV. (b) Vertical line scan through the simulated voltage distribution around a localized shunt for different shunt resistances R_P with fixed sheet resistivity $\rho_{sh} = 40\,\Omega/\square$ and (c) different sheet resistivities ρ_{sh} for fixed shunt resistance $R_P = 160\,\Omega$. All simulations have been performed under 1 sun illumination, open circuit conditions, and a dark saturation current density $J_{01} = 10^{-12}$ A/cm^2, contact resistivity 3 mΩ cm^2, metallization resistivity $3.2 \times 10^{-6}\,\Omega$ cm, short circuit current density 36 mA/cm^2, second diode saturation current density $J_{02} = 10^{-8}$ A/cm^2. The simulated fill factors in (a) for $\rho_{sh} = 40\,\Omega/\square$ and shunt resistances of 40 Ω, 160 Ω, and 640 Ω are 69.8%, 76.8%, and 79.7%, respectively

DOI: 10.1002/pip

$\exp(eV_{xy}/kT)$ with $kT/e = 25$ mV, neglecting the complexities in the relation between local junction voltage and PL signal discussed in Section 'Luminescence imaging'. An EL image would also exhibit a similar blurred intensity dip around the position of the shunt as can be concluded from Figure 5a.

Figure 3b quantitatively shows for the case of an illuminated cell, that the depth and the lateral extension of the voltage dip shrink with growing shunt resistance. Figure 3c shows the voltage dip around a shunt for different sheet resistivities under irradiation. The higher the sheet resistivity, the smaller is the current drained from the surrounding non-shunted areas. A smaller current through the shunt causes a smaller voltage drop across the shunt resistance and therefore a smaller local junction voltage at the shunt position. The voltage dip becomes deeper and narrower toward higher sheet resistivities. The case simulated with $\rho_{sh} = 1\ \Omega/\square$ is unrealistic for typical emitters, but it shows that the depth of the voltage dip shrinks on the cost of a ''wide-distance'' voltage drop toward low sheet resistivities.

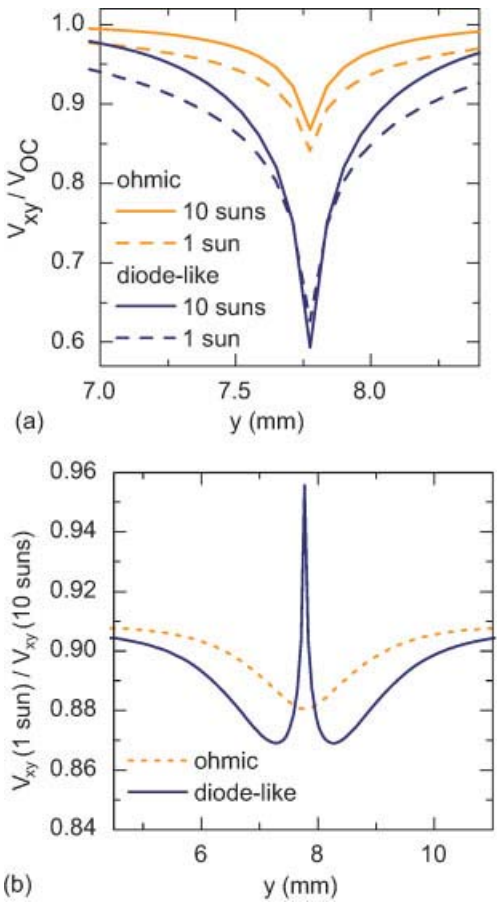

Figure 4. (a) Simulated vertical line scans through the open-circuit voltage distributions around an ohmic and a diode-like shunt with ideality factor of two at different irradiation intensities normalized to the respective open-circuit voltage. (b) Division of the voltage distribution obtained for 1 sun and for 10 suns irradiation intensity for an ohmic and a diode-like shunt, respectively. An ohmic shunt and a diode-like shunt differ significantly in shape in this representation

The shape and depth of the voltage dip around a shunt is a measure for the shunt resistance, as long as the series resistance in the vicinity of the shunt is known and the diode-properties are laterally homogeneous in this area. One might conclude, that this information could allow for the quantification of shunt resistances from luminescence images, at least for mono-crystalline silicon solar cells, once the luminescence images are calibrated on voltages. However, at present it seems difficult to obtain accurate information on the local properties around a shunt, especially as the effective series resistance varies significantly over the cell. Section 'Shunts under the metallization and remote shunts', for example, will show that the position of the shunt relative to the grid lines has a great influence on the shape of the voltage dip.

Injection-level dependent measurements—distinguishing ohmic and diode-like shunts

Getting information about the current–voltage characteristics of a shunt is not straight-forward with EL and PL imaging. While dark and illuminated lock-in thermography allow for a distinction between ohmic shunts and diode-like shunts by simply comparing a measurement at forward bias with a measurement at reverse bias, such a procedure is impossible with luminescence imaging. An EL image of a cell under reverse bias shows no luminescence signal due to band-to-band recombination, as can be concluded from Figure 1b. For PL images we have also shown in Figure 1b that the luminescence signal does not follow the junction voltage toward low values.

However, based on our simulations we found that it might be possible to get information about the current–voltage characteristics of a shunt by comparing the shape of the voltage dip between two images taken at different injection levels. Different injection level means different light intensity for PL and different electrical current density for EL, respectively. Figure 4 shows that the shape of the voltage dip around an ohmic and a diode-like shunt changes with injection

DOI: 10.1002/pip

level. The change in shape is different for ohmic and diode-like shunts. Dividing the voltage distribution obtained at 1 sun irradiation intensity by the voltage distribution obtained at 10 suns, for example, yields a plot where the shunt-affected region differs significantly between the ohmic and the diode-like case. Figure 4b shows that the diode-like shunt exhibits a sharp peak at the position of the shunt in this plot. Simulations show that the exact shape of this peaked curve depends on the shunt diode ideality factor, but also on the properties of the environment which makes it difficult to obtain an ideality factor of the shunt diode by this method. The existence of a peak as a distinctive feature indicating a diode-like shunt, however, appears to be independent of the properties of the environment according to our simulations. Figure 5 illustrates a similar behavior for the dark case under current injection. Whether these features may be qualitatively and quantitatively resolved by EL or PL imaging remains to be tested. Unfortunately, the features of Figure 4b and Figure 5b do not appear in the difference of the line scans which would be easier to access experimentally.

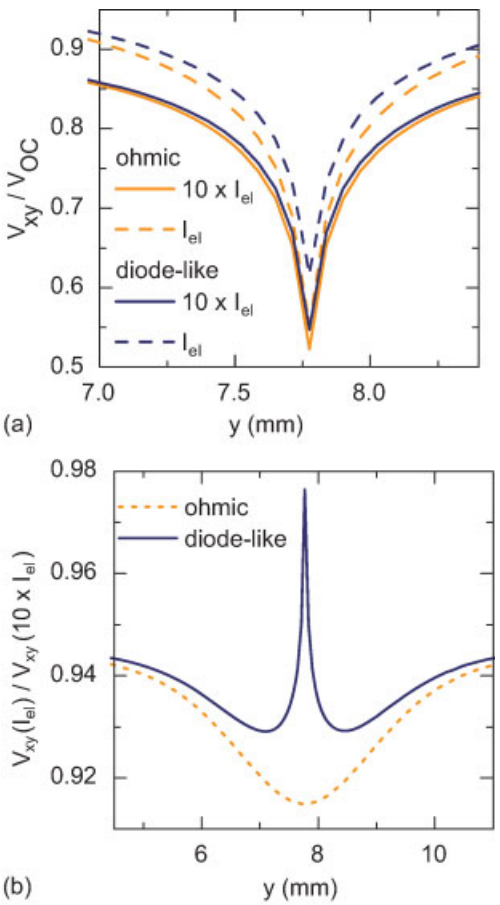

Figure 5. (a and b) Simulation results like in Figure 4 but simulated for the dark case under current injection with current densities of $I_{el} = 51.5$ mA and $10 \times I_{el}$ which corresponds approximately to the short circuit current at 1 sun and 10 suns, respectively

Shunts under the metallization and remote shunts

Figure 6a and b illustrate the influence of the position of the shunt relative to the metallization on the voltage distribution for the case of an illuminated cell under open-circuit conditions. The voltage dip around a shunt *under* a finger is significantly smaller than the dip around a shunt *between* two fingers. The reason is simply that the shunt below the grid can drain a high current from the entire cell through the lowly resistive metal grid. The current drained from the direct vicinity is thus very small and so is the local voltage dip which is the important feature for shunt detection with PL imaging. Figure 6c and d show that this effect is also observable in the case of current injection in the dark which represents the conditions in EL imaging.

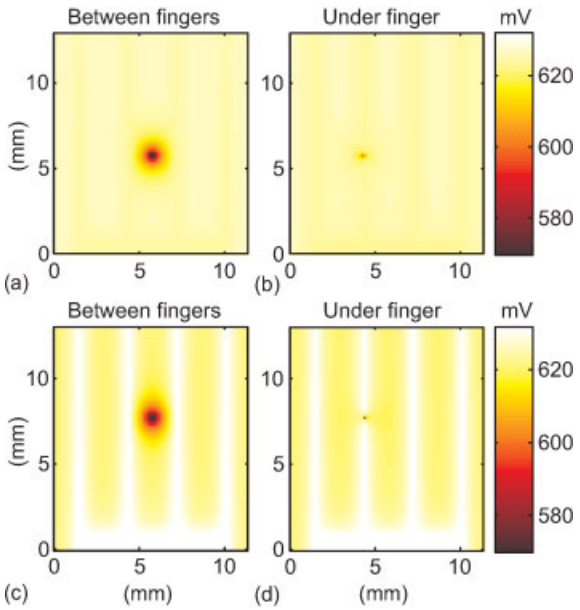

Figure 6. Simulation of the shape of the voltage dip for different shunt positions under (a and b) illumination and open-circuit conditions, and for (c and d) dark current injection of 51.5 mA which corresponds approximately to the short circuit current at 1 sun illumination. The shunt resistance was 160 Ω and the sheet resistivity was 40 Ω/□

DOI: 10.1002/pip

To illustrate this effect in practice, we introduced shunts into mono-crystalline silicon solar cells which were produced in a typical industrial process. The shunts have been laser-fired into the fingers and into the middle between the fingers. Figure 7 shows an ILIT image and a PL image of such a cell, both taken under open-circuit conditions. The ILIT image, which shows the power dissipated in the shunt, exhibits a strong signal for the shunts *below* the grid fingers (labeled A–E). The PL image, however, is only weakly influenced by these shunts. The shunts *between* grid lines (labeled 1–7), in contrast, cause significant changes in the PL image and tend to appear weaker in the displayed ILIT image. Especially shunts 1, 2, and 7 show up only faintly in this ILIT image.

The measurements and simulations show a limitation of PL imaging for shunt detection (that holds also for Corescan[17]): shunts that are located under the metallization are only weakly detectable by PL imaging. Unfortunately, shunts in these areas have a high impact on fill factor and efficiency.[24] Only if shunts under the metallization have very low resistance values, they influence the PL image as well. In this case, the shunt drains a high current from large parts of the cell, causing a blurred wide-area voltage drop toward the shunt position like the one observed in Reference 3.

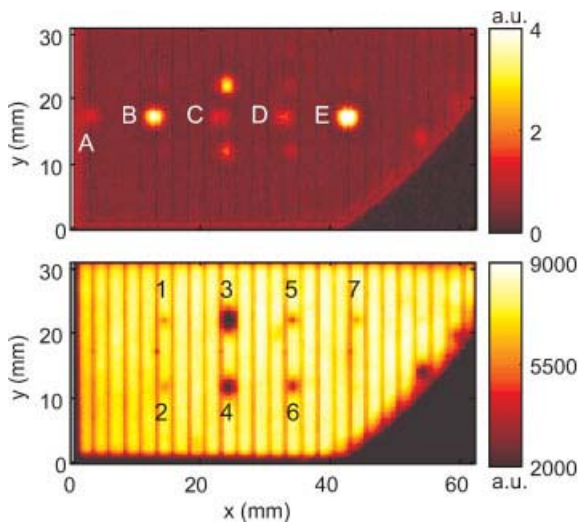

Figure 7. ILIT (top) and PL (bottom) measurements of an intentionally shunted solar cell under open-circuit conditions. Shunts on grid lines are labeled by letters A–E in the ILIT image, while shunts between grid lines are labeled by numbers 1–7 in the PL image. Shunts appear as high values in ILIT and low values in PL imaging. The shunts have been introduced by laser firing

Despite these limitations, the measurements and simulations also show that PL imaging is particularly sensitive to "remote" shunts which are surrounded by high series resistances. An application, where PL could be promising in the light of this discussion, is the assessment of laser edge isolation quality. With ILIT, for example, we recently had difficulties to quantitatively assess losses in laser edge isolation on industrial solar cells for global shunt resistivities above approximately $1000\,\Omega\text{cm}^2$. Whether PL imaging is more sensitive than ILIT for this application remains to be tested.

CONCLUSIONS

Shunts can be detected by EL and PL imaging because the luminescence signal is related to the local junction voltage. Majority carrier currents drained by a shunt cause a voltage dip in the vicinity of the shunt which is visible in luminescence images. Depth and lateral extension of the voltage dip depend on the shunt resistance and the surrounding series resistances. A quantification of the shunt resistance via this effect relies firstly on an accurate voltage calibration of luminescence images around localized shunts which we showed is non-trivial. Secondly, we showed that the position relative to the metallization strongly influences the effective series resistances around the shunt which makes it additionally difficult to assess the influence of the shunt on the global current–voltage curve.

Weak and moderate shunts under fingers are only weakly detectable by luminescence imaging. Only for very low shunt resistances do these shunts significantly affect the luminescence image, but are then difficult to localize due to a strong blurring.

On the other hand, PL imaging is very sensitive to shunts which are surrounded by high lateral series resistances. This property could turn out to be particularly useful for the determination of laser edge isolation quality, in a production line as well as off-line.

Acknowledgements

Fruitful discussions with P. Würfel and M. Hermle are gratefully acknowledged. The authors from Fraunhofer ISE and University of Freiburg acknowledge support by the German Federal Ministry of Education and Research under Contract No. 01SF0401 (NETZ DIAGNOSTIK). The Centre of Excellence for Silicon Photovoltaics and Photonics is supported under the Australian Research Council's Centres of Excellence Scheme.

DOI: 10.1002/pip

REFERENCES

1. Trupke T, Bardos RA, Schubert MC, Warta W. Photoluminescence imaging of silicon wafers. *Applied Physics Letters* 2006; **89**: 044107.
2. Fuyuki T, Kondo H, Yamazaki T, Takahashi Y, Uraoka Y. Photographic surveying of minority carrier diffusion length in polycrystalline silicon solar cells by electroluminescence. *Applied Physics Letters* 2005; **86**: 262108.
3. Kasemann M, Schubert MC, The M, Köber M, Hermle M, Warta W. Comparison of luminescence imaging and illuminated lock-in thermography on silicon solar cells. *Applied Physics Letters* 2006; **89**(22): 224102.
4. Bothe K, Pohl P, Schmidt J, Weber T, Altermatt P, Fischer B, Brendel R. Electroluminescence imaging as an in-line characterisation tool for solar cell production. *Proceedings of 21st European Photovoltaic Solar Energy Conference and Exhibition*, 2006; Dresden (Germany).
5. Trupke T, Bardos RA, Abbott MD, Fisher K, Bauer J, Breitenstein O. Luminescence imaging for fast shunt localization in silicon solar cells and silicon wafers. *International Workshop on Science and Technology of Crystalline Si Solar Cells*, 2006; Sendai (Japan).
6. Breitenstein O, Rakotoniaina JP, Kaes M, Seren S, Pernau T, Hahn G, Warta W, Isenberg J. Lock-in thermography—a universal tool for local analysis of solar cells. *Proceedings of the 20th European Photovoltaic Solar Energy Conference*, 2005; Barcelona (Spain).
7. Isenberg J, Heide ASHvd, Warta W. Range of loss mechanisms accessible by illuminated lock in thermography (ILIT). *Proceedings of the 20th European Photovoltaic Solar Energy Conference*, 2005; Barcelona (Spain).
8. Isenberg J, Warta W. Realistic evaluation of power losses in solar cells by using thermographic methods. *Journal of Applied Physics* 2004; **95**(9): 5200–5209.
9. Isenberg J, Warta W. Spatially resolved evaluation of power losses in industrial solar cells by illuminated lock-in thermography. *Progress in Photovoltaics: Research and Applications* 2004; **12**(5): 339–353.
10. Kaes M, Seren S, Pernau T, Hahn G. Light-modulated lock-in thermography for photosensitive pn-structures and solar cells. *Progress in Photovoltaics: Research and Applications* 2004; **12**(5): 355–363.
11. Breitenstein O, Langenkamp M. *Lock-in Thermography—Basics and Use for Functional Diagnostics of Electronic Components*. Springer Verlag: Berlin/Heidelberg, 2003.
12. Würfel P. *Physics of Solar Cells: from Principles to New Concepts*. Wiley-VCH: Weinheim, 2005.
13. Trupke T. Influence of photon reabsorption on quasi-steady-state photoluminescence measurements on crystalline silicon. *Journal of Applied Physics* 2006; **100**(6): 063531.
14. Trupke T, Bardos RA, Abbott MD, Cotter JE. Suns-photoluminescence: contactless determination of current–voltage characteristics of silicon wafers. *Applied Physics Letters* 2005; **87**: 093503.
15. Clugston DA, Basore PA. PC1D Version 5:32-bit Solar Cell Modeling on Personal Computers. *26th IEEE PVSC*, 1997; Anaheim (USA).
16. Trupke T, Pink E, Bardos RA, Abbott MD. Spatially resolved series resistance of silicon solar cells obtained from luminescence imaging. *Applied Physics Letters* 2007; **90**(9): 093506.
17. Breitenstein O, Rakotoniaina JP, Heide ASHvd. Shunt detection in solar cells with the Corescanner and lock-in thermography: a comparison. *Proceedings of the 11th NREL Workshop on Crystalline Silicon Solar Cell Materials and Processes*, 2001; Estes Park (Colorado, USA).
18. van der Heide ASH, Bultman JH, Hoornstra J, Schönecker A, Wyers GP, Sinke WC. Locating losses due to contact resistance, shunts and recombination by potential mapping with the Corescan. *Proceedings of the 12th NREL Workshop on Crystalline Silicon Solar Cell Materials and Processes*, 2002; Breckenridge (Colorado, USA).
19. van der Heide ASH, Schönecker A, Wyers GP, Sinke WC. Mapping of contact resistance and locating shunts on solar cells using resistance analysis by mapping of potential (RAMP) techniques. *Proceedings of the 16th European Photovoltaic Solar Energy Conference*, 2000; Glasgow (UK).
20. Breitenstein O, Rakotoniain JP. Electrothermal simulation of a defect in a solar cell. *Journal of Applied Physics* 2005; **97**: 074905.
21. Köber M, Hermle M, Isenberg J, Kasemann M, Cárdenes H, Warta W. Analysis of effects caused by parameter inhomogeneities with a 2-D-modelling tool based on circuit simulation. *21st EC-PVSEC*, 2006; Dresden (Germany).
22. Galiana B, Algora C, Rey-Stolle I, Vara IG. A 3-D model for concentrator solar cells based on distributed circuit units. *IEEE Transactions on Electron Devices* 2005; **52**(12): 2552–2558.
23. Grabitz PO, Rau U, Werner JH. Modeling of spatially inhomogeneous solar cells by a multi-diode approach. *physica status solidi (a)* 2005; **202**(15): 2920–2927.
24. Dicker J, Isenberg J, Warta W. Effect of shunt distribution on the overall solar cell performance investigated by circuit simulation. *Proceedings of the 17th European Photovoltaic Solar Energy Conference*, 2001; Munich (Germany).
25. Engelhardt M. LTSpice/SwitcherCAD III. 2007, Linear Technology Corporation.
26. Würfel P, Trupke T, Puzzer T, Schaffer E, Warta W, Glunz SW. Diffusion lengths of silicon solar cells from luminescence images. *Journal of Applied Physics* 2007; **101**(12): 123110.

DOI: 10.1002/pip